IEEE Access
Multidisciplinary | Rapid Review | Open Access Journal

Received 16 June 2022, accepted 29 June 2022, date of publication 4 July 2022, date of current version 14 July 2022.

*Digital Object Identifier 10.1109/ACCESS.2022.3188247*

RESEARCH ARTICLE

# Experimental Demonstration and Evaluation of BCH-Coded UWOC Link for Power-Efficient Underwater Sensor Nodes

**MAAZ SALMAN, JAVAD BOLBOLI, AND WAN-YOUNG CHUNG, (Senior Member, IEEE)**
Department of Artificial Intelligence Convergence, Pukyong National University, Nam-gu, Busan 48513, Republic of Korea

Corresponding author: Wan-Young Chung (wychung@pknu.ac.kr)

This work was supported by the National Research Foundation of Korea (NRF) funded by the Korean Government [Ministry of Science and ICT (MSIT)] under Grant 2020RIA4A1019463.

**ABSTRACT** Mobile nodes can encounter many challenges in underwater environments during communication due to turbidity, suspended particles, small bubbles, and turbulence. These factors cause absorption and scattering, ultimately corrupting optical signals. Error-correcting codes can be used to correct certain corrupted bits and thus reduce the errors in a channel. In this work, a Bose-Chaudhuri-Hocquenghem (BCH) (31, 16)-coded underwater wireless optical communication (UWOC) system is proposed to enhance the communication performance between power-efficient sensor nodes. The proposed BCH-coded system needs a reasonable amount of computing capability and is powered by a battery, enabling the node to have an on-site data processing unit and untethered communication. The encoder and decoder algorithms of the BCH code are implemented on the Embedded C software and coded to run on an Atmel ATmega128A micro-controller. The system's performance is evaluated by emulating the effects of scattering and absorption, noise due to surrounding and ambient light, turbidity, air bubbles, and turbulence in a natural underwater environment. Moreover, a 0.5 Mbps BCH-coded link achieves a 93.5% PSR, which is 6% better than that of the uncoded system, at a moderate turbidity level of 64 NTU, in the presence of weak turbulence (induced by a pump at a 2.5 $L/min$ displacement rate) and air bubbles (generated by an aerating jet at an airflow rate of about 1.2 $L/min$).

**INDEX TERMS** Underwater wireless optical communication (UWOC), BCH code, scattering, turbulence, turbidity.

## I. INTRODUCTION

Underwater wireless communication promises an array of applications of untethered seafloor environment monitoring systems for tracking, monitoring, and analyzing different fish behaviors [1]. An underwater local area network requires mobile sensor nodes, which makes tethered links infeasible and intrusive. The susceptibility of radio-frequency waves in water leads to severe attenuation, preventing their large-scale deployment and application. Although sound waves are a viable alternative due to their small attenuation in underwater channels [2], [3], their limited bandwidths, long propagation delays, low data rates, and bulky components hinder their application for mobile underwater nodes [4], [5]. Furthermore, the complex environments of water channels impose many challenges. Communication systems using acoustic [2], [6], electromagnetic, and optical [7], [8] waves overcome the fundamental barriers of underwater wireless communication, but they still have disadvantages and challenges [9]. Optical wireless communication is drawing the attention of many researchers due to its high data transfer rates, low cost, low latency, and wide spectrum [8], [9]. Figure 1 shows a block diagram of a UWOC system that uses a light-emitting diode (LED) as an optical source and an avalanche photodiode (APD) to detect optical signals at the receiver [10].

The message is modulated and transmitted across the water channel by driving the optical source (the LED) at the transmitter (Tx). The photodetector detects the received

The associate editor coordinating the review of this manuscript and approving it for publication was Yougan Chen.

**TABLE 1. Summary of literature on UWOC error-correcting codes.**

| Literature | Channel Code | Theoretical Analysis/ Experiment | Distance | Tethered / Untethered | Data / Signal Processing | Mobility | Complexity |
|---|---|---|---|---|---|---|---|
| [45] | RS, CRC, LT | Theoretical analysis and Experiment | 50 m | Tethered | Off Node | ✪ | High |
| [43] | RS, BCH | Theoretical analysis | 10 m | Tethered | Off Node | ✪ | High |
| [14] | RS, CRC, LT | Experiment | 25 m | Tethered | Off Node | ✪ | High |
| [46] | RS | Experiment | 7.7 m | Tethered | Off Node | ✪ | High |
| [36] | CRC | Theoretical analysis and Experiment | 5 m | Tethered | Off Node | ✪ | High |
| [47] | LDPC and Turbo | Experiment | 2 m | Tethered | Off Node | ✪ | High |
| [44] | BCH | Theoretical analysis and Experiment | 5 m | Tethered | Off Node | ✪ | High |
| [30] | RS | Theoretical analysis and Experiment | 3.66 m | Tethered | Off Node | ✪ | High |
| Proposed work | BCH | Experimental | 4 m | Untethered | On-Node | ☑ | Low |

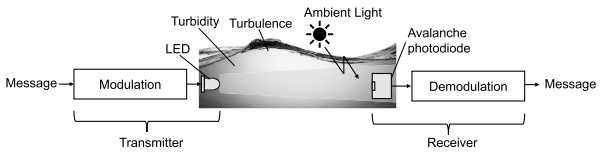


**FIGURE 1. Block diagram of UWOC system using LED and APD.**

optical signal and deciphers the message via demodulation at the receiver (Rx). However, the modulated optical beam encounters many physical obstacles, such as turbulence due to water waves, hanging particles (such as chlorophyll particles), water bubbles, and bright ambient light. These factors play a major role in the high absorption of optical signals, scattering, and high ambient light, which ultimately reduce system performance and the signal-to-noise ratio [11].

Unlike free-space optical communication, underwater optical communication channels involve different variables. Moreover, for an underwater optical beam, the propagating wave encounters more obstacles (and thus higher attenuation) than a free-space link, and the scattering and absorption of optical signals in underwater environments are major factors. The absorption in such a medium reduces the photon count, and the scattering effect deflects the optical beam from the desired path, reducing the light intensity at the receiver end. These disturbances cause beam attenuation and fluctuations in the signal's intensity, resulting the received packets with the addition of bit or burst errors, which ultimately corrupt the original data. Optimum number of corrupted bits can be corrected using smart algorithms, called forward error correction codes. These codes use redundant bits to recover the bit error(s) in the received packet. Table 1 lists notable past works in the area of error-correcting codes for underwater optical communication systems. In these works, data processing or signal processing tasks, such as the encoding and decoding of message bits, were performed on separate PCs using physical connections (Ethernet and coaxial cables) between the nodes (transmitters or receivers) and the PCs. This work focuses on a small underwater sensor network that has specified design constraints and functions in terms of size and mobility requirement in a particular environment as sensor nodes. These requirements mean that a sensor node should comprised of components which are compact in size, non-invasive, and consume less power. Hence, there is a trade-off between the transmission rate and the size of the sensor node. Furthermore, the proposed system is designed for SMPs, such as those used for fish monitoring in smart fish farms, compact communication devices for divers, and remote tracking and monitoring of marine lives in offshore fish farms, which require a node to be power-efficient and compact.

This work demonstrates the performance of a forward error correction scheme-enabled UWOC link in different levels of pure, clean water and turbid water in a water tank with a volume of $4 \times 0.5 \times 0.5\ m^3$. The experiments involve varying wavelengths of the optical signal at different data rates and with various distances between the transmitter and the receiver in the presence of ambient light and turbulence. The proposed Bose-Chaudhuri-Hocquenghem (BCH) error-correcting code improves the performance of

a UWOC system by mitigating the effects of scattering and turbulence.

## II. LITERATURE REVIEW

A large number of studies have explored the design and development of reliable, high-speed optical communication systems and expanded their application to underwater environments by deploying, testing, and evaluating UWOC systems for various applications. UWOC systems have diverse uses. [12], [13] addressed the feasibility of, and challenges encountered by, underwater Internet of Things (UIoT) systems in developing various applications, such as fish farms, diver network monitoring, and early warning systems. Robust real-time underwater audio and video streaming is implemented using wireless optical communication for underwater uses [14], [15]. Furthermore, UWOC is established for real-time marine observation, diver communication, and ocean monitoring [16]–[18].

Some studies [9], [19]–[22] show that the optical wavelength in the range of 450-500 nm (blue and green LEDs) is the most suitable (only minimally affected by scattering and absorption) for pure seawater or clear water. Furthermore, due to turbulence and bubbles in underwater media, beam fluctuations occur, which in turn increase attenuation [23], [24]. Past studies [25], [26] addressed the performance of UWOC systems in turbid water channels using water tank experiments with varying amounts of the antacid Maalox. An LED-powered UWOC was designed for affordable, stable, compact wireless optical communication for small mobile platform (SMP) applications and demonstrated in a highly turbid outdoor channel [27]. Experiment-based studies [28], [29] have found a reciprocal effect of turbulence caused by the presence of induced turbulence and air bubbles. In [30], Reed-Solomon (RS) codes were utilized in a UWOC system to mitigate the effects of channel turbidity with varying attenuation coefficients. An optical communication interface was presented in [15]; the interface consisted of a transmitter interface with an on-board field-programmable gate array (FPGA), micro-controller, and LED transmitter. The FPGA could perform error correction encoding (RS) and interfacing with any sensor node. In [31], the authors proposed a UWOC system that employs RS and low-density parity check codes to mitigate the effect of attenuation due to turbulence in water. With the exception of [15], previous works on UWOC systems enabled by forward error correction schemes focus on increasing system data rates using highly sophisticated yet bulky and expensive components [32]–[37]. These systems use off-board computing units for data processing tasks, such as encoding, decoding, and signal processing. These systems are particularly designed for large-scale applications, such as submarine, UAV, and seafloor monitoring, real-time high-quality video streaming, and imaging systems [36], [38]–[42].

The design characteristics of the proposed system are compared with those in related works in table 1. The table demonstrates that the proposed system has an edge in signal processing (software-based encoding, decoding, and modulation) on the node, which eliminates the need for a data cable (untethered). Additionally, the transmitter is battery powered, thereby enabling the transmitter interface to perform as a mobile node. These properties can benefit UIoT applications that require mobility and power efficiency. The performance of BCH and RS codes was compared in a purely theoretical analysis work via Matlab simulations [43]. In [44], the performance of a BCH-coded link was analyzed. Although the experimental results showed good performance, data computation (i.e., encoding and decoding) was performed on Matlab using a remote PC. The encoded data streams were stored in a flash memory and transmitted across the water channel via an FPGA. The received data were recovered at the receiver, and signal processing and decoding were performed using Matlab. Therefore, the present work has advantages over other works [43], [44] in a range of areas, such as the successful implementation and demonstration of the proposed system through a series of experiments. Furthermore, the system is powered by a battery and has an on-board computing unit, which provide mobility to the sensor node. The proposed system also exhibits low complexity regarding its circuit, its dimensions, and the number of components required to address its computing needs.

## III. CONTRIBUTIONS

In this work, a forward error correction scheme-enabled UWOC system is proposed and then implemented and evaluated under different emulated underwater environmental conditions. We provide a proper gateway for creating an interface that accommodates stable, compact, affordable, reliable communication for SMP applications by testing the proposed LED-powered, BCH-coded UWOC system in water with different levels of turbidity in the presence of surrounding and ambient light and channel turbulence induced by waves and air bubbles. This work contributes to the field of study in this domain as follows:

- A software-based BCH scheme is coded on Embedded C and implemented on a small micro-controller unit MCU) to function on a small-sized interface for SMP applications. Mobility is achieved by powering the system with a small 5 V Li-Po battery, which enables the node interface to facilitate power-efficient, untethered communication.
- The system is equipped with ATMega128 micro-controller with a small energy footprint. The operating voltage and current of the ATmega128 are 2.7-5.5 V, and 3-15 mA, respectively. Moreover, the micro-controller only consumes about 7 $\mu$A in a power save mode. The output power of LED sources, blue and red, are 102 and 72 mW, respectively. These characteristics of total low power consumption catapult the proposed system's suitability for power efficient, compact SMP applications.
- The system is evaluated in a variety of emulated underwater environments to check the performance,

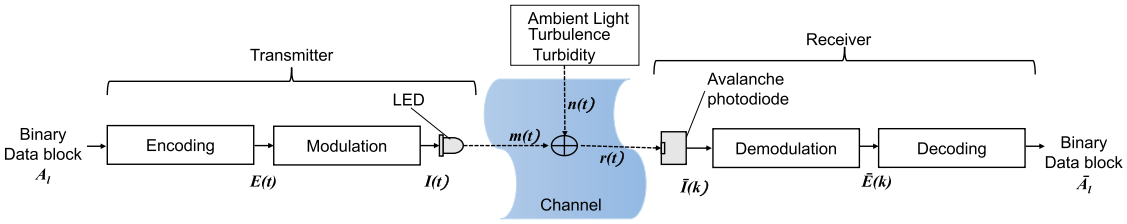


**FIGURE 2.** Block diagram of BCH-coded UWOC system.

reliability, and feasibility of the BCH-coded communication link.

- Although 25% of packets are lost in the presence of strong ambient and surrounding light (about 830 lux) and turbulence (induced by a pump at a 5 L/min displacement rate), the BCH-coded link improves the PER performance by about 16% at a data rate of 28.8 Kbps.
- The system is evaluated in extremely and moderately turbid water. These experiments are conducted to evaluate its performance under the accumulated effects of different turbidity levels, surrounding and ambient light, and turbulence induced by artificially generated waves and air bubbles. The system can communicate in clean water with a 10% PSR improvement within a link range of 2 m under high ambient light (about 1550 lux), turbulence induced by the pump at a 5 L/min displacement rate, and air bubbles generated by an aerating jet at an airflow rate of about 2.5 L/min.
- The system maintains successful communication within a link range of about 1 m, with a 13% PSR improvement in highly turbid water (about 305 NTU) and the other induced disturbances discussed above.
- A 4 m BCH (31, 16)-coded UWOC link achieves a 93.5% PSR at a data rate of 0.5 Mbps, with a PSR improvement of 6% in moderate-turbidity water (64 NTU) in the presence of turbulence induced by the pump at a 2.5 L/min displacement rate, and air bubbles generated by the aerating jet at an airflow rate of about 1.2 L/min.

## IV. SYSTEM MODEL

The data stream to be transmitted is modulated with on-off keying (OOK) with LED sources with wavelengths of 470 and 665 nm. A multi-function water pump generates turbulence and small bubbles in the water. Zinc oxide powder is used to simulate turbidity, and the turbidity level is changed by modifying the powder concentration in the water. Turbidity is then measured using a turbidity meter. The transmitter section, or sensor node, is enclosed in a transparent watertight (IPV7) box and moved in the water tank to vary the distance between the transmitter and the receiver, and the effects of the different distances on system performance are evaluated. Received light with wavelengths of 470 and 665 nm is captured using a multi-pixel photon counter-APD (MPPC-APD) and a Si-PIN photodiode with operating bandwidths of 450-550 and 600-700 nm, respectively. Light intensity is converted into an electrical signal using a suitable trans-impedance electric circuit. Modulation, demodulation, encoding, and decoding are implemented in an Atmel ATmega128A MCU. Figure 2 shows a block diagram of the proposed UWOC system, which employs a BCH error-correcting code with modulation, where $A_l$, $E(t)$, and $I(t)$ represent the transmitted binary bit stream, BCH-encoded data, and modulated data, respectively. The detected optical signal $r(t)$ becomes a combination of the original signal $m(t)$ and the noises $n(t)$ after it passes through the noisy water channel. The receiver consists of the BCH decoder, demodulation section, and receiving trans-impedance circuit; $\bar{I}(k)$, $\bar{E}(k)$, and $\bar{A}_l$ represent the converted voltage from the received light intensity, received data after demodulation, and BCH-decoded data (or final estimated message), respectively.

## V. EXPERIMENTAL SETUP

The major components of the proposed UWOC system are discussed below.

### A. LED

Underwater environments show minimal attenuation of light operating in the frequency bandwidth of 470-550 nm [48]. Therefore, two LEDs with wavelengths of 470 nm (blue, G05BC09-2) and 660 nm (red, G05RC18 ) are used to optically modulate the signal to transmit the data through the medium and assess the performance of the system. The blue and red LED sources have a maximum luminous intensity of 2500 mcd and output power of 102 and 72 mW, respectively. The two LEDs are used separately in two experiments to evaluate their individual performance.

### B. PHOTO-DIODE

A Si-PIN photodiode (S5107) with a spectral response of more than 50% for an optical source of 700-1050 nm is employed to detect the red LED optical signal (wavelength of $\lambda = 730$ nm). An MPPC photodiode (S13360), with a 50% photon detection efficiency within the operating bandwidth of 400-500 nm, is used to detect the blue LED optical signal ($\lambda = 470$ nm) to recognize the transmitted optical signal.

### C. ATmega128A MICRO-CONTROLLER

The ATmega128A MCU is utilized to execute different BCH codes and modulation functions. The micro-controller is powered with a 5 V Li-Po battery to enable and maintain the mobility of the sensor node. The operating voltage and current of the ATmega128A are 2.7-5.5 V, and 3-15 mA, respectively. The Atmega128A only consumes about 7 $\mu$A of current in a power save mode. Furthermore, untethered communication of the mobile sensor node is enabled by running the modulation technique and other functions, such as the encoding of message bits into BCH-coded bits on the micro-controller.

### D. TRANSMITTER CIRCUIT

The transmitter circuit is comprised of analog comparator (LM393) and NPN bipolar junction transistor (2N3904). These components are used to compare and switch the electrical signal to form a smooth digital pulses which drive the LED to formulate corresponding optical pulses. The circuit diagram of the transmitter circuit is illustrated in figure 6.

### E. TRANS-IMPEDANCE AMPLIFIER (TIA) BASED OPTO-RECEIVER

The receiver circuit consists of buffer (TL082), amplifier (TL082), comparator (LM393), and $-5$V generator (LMC7660). A continuous feeble opto-to-electric signal is collected by the voltage follower buffer section, the signal is further amplified up-to 100 times by the TL082 amplifier, then fed to LM393 for transistor–transistor logic (TTL) comparison (0 or 5 V). The LMC7660 IC is used to generate $-5$ V to accommodate the functions of buffer and amplifier. The circuit diagram of the TIA based receiver circuit is shown in figure 6.

### F. MODULATION

The experiments are performed using intensity modulation / direct detection (IM/DD) to reduce system complexity. Non-return-to-zero OOK (NRZ-OOK) is the most applicable modulation technique for this purpose due to its efficient, straightforward approach. First, the data stream is modulated in pulses. Then, the presence of the pulse is decoded as binary one, and its absence is interpreted as binary zero.

### G. UNDERWATER CHANNEL

An underwater medium is composed of various molecules and impurities. The passage of light through these molecules causes changes in the refractive index. The light beam refracts, deviates, or deflects from its original path. This deviation causes a scattering effect, whereas the reduction in optical beam intensity for phytoplankton decreases the light intensity for photosynthesis. Attenuation is an additive quantity of optical loss due to absorption and scattering effects [49]. The effects of scattering and absorption are at the minimum at wavelengths of 470-530 nm (blue and green) [44]. Furthermore, turbulence in an underwater channel can cause optical signal scintillation, whereas absorption and scattering further degrade the quality of optical signals. In the experiments in this study, a multi-function water jet induces turbulence in the underwater channel. The attenuation effect depends on the characteristics of the underwater medium; these characteristics are deterministic constants obtained using the Beer-Lambert law for specific medium types, whereas the impact of turbulence on an optical beam has a random nature and can be obtained using the probabilistic expressions shown in [50]. The experimental setup is shown in figure 3.

### H. TURBIDITY

ZnO powder is added to the water to emulate the turbidity in natural environments, and the turbidity level is changed by modifying the powder concentration [51]. The turbidity of the tested water is measured using the Arduino Gravity turbidity sensor SKU SEN0189, which measures water quality by determining the level of turbidity (or opaqueness). It detects particles suspended in water by measuring light transmittance and scattering rates, which change with the concentration of total suspended solids (TSS) in water. The turbidity of clear water is assumed 0.09 NTU. The turbidity of drinking water is less than 1 NTU, and, according to most US states' regulations, ocean water turbidity should not exceed 50 NTU [52]. The relationship between the measured turbidity level (TU), transmittance (T), and absorbance (A) for different concentrations (C) of ZnO are shown in table 2 [51]. Furthermore, the relationship between the beam attenuation coefficient (c) and turbidity levels of different water types are plotted in figure 5. The scatter data plot represented by blue triangles in the figure have been reported in [53]. These data are computed to derive the regression line to confirm the linearity between the two parameters. The corresponding turbidity levels, and attenuation coefficients with respect to attenuation coefficients mentioned in [54], [55] (commonly used conventional method to determine different water types i.e. clear, coastal, harbor, harbor 1, harbor 2), and turbidity levels used in this work, respectively are calculated using the achieved linear proportionality.

### I. EXPERIMENT BOX

A customized transparent waterproof box is designed and fabricated to enclose the transmitter components during the underwater experiments. The transmitter components, i.e. AtMega128A, transmitter circuit, 5 v Li-Po battery, plano-convex lens, and the optical source (LED) are installed in the water tight transparent box. A variable gimbal system is installed in the box to align and focus the optical signal in a certain direction with a constant luminous intensity, and enhance the range of the optical signal. The experiment box is shown in figure 4.

## VI. BCH CODE

Multiple factors, such as absorption, scattering, and turbulence, play a crucial role in the attenuation and scintillation

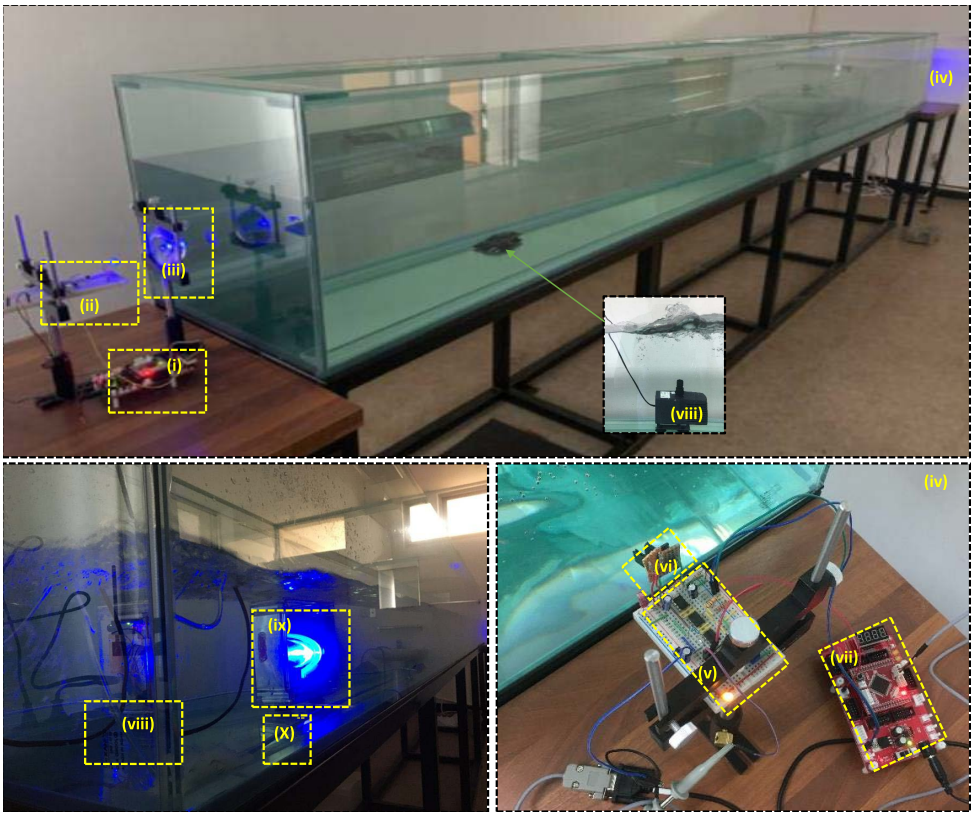


**FIGURE 3.** Experimental setup of BCH-coded UWOC system: (i) micro-controller (Atmel ATmega128A) used for encoding and modulation, (ii) driver circuit and optical source (LED), (iii) collimating lens, (iv) receiver unit, (v) receiver circuit, (vi) photodetector (MPPC-APD), (vii) micro-controller (Atmel ATmega128A) used for decoding and demodulation, (viii) water pump (for inducing waves), (ix) transmitter enclosed in waterproof box, (x) small tubes for air bubbles.

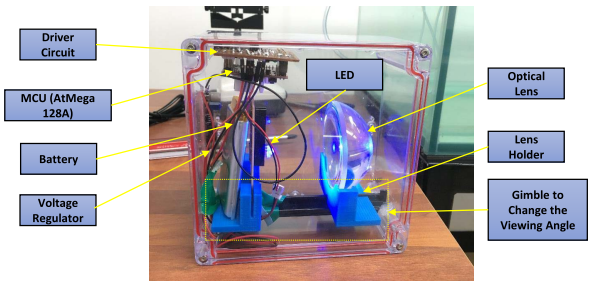


**FIGURE 4.** Waterproof experiment box.

**TABLE 2.** Optical properties of water, namely, turbidity level (TU), transmittance (T), and absorbance (A) for different ZnO concentrations (C) [51].

| TU (NTU) | T (%) | A ($m^{-1}$) | C ($g/m^3$) |
|---|---|---|---|
| 0.09 | 89.1 | 5.00 | 0 |
| 0.36 | 88.4 | 5.41 | 16.78 |
| 1.71 | 87.0 | 6.01 | 33.57 |
| 25.42 | 85.3 | 7.00 | 67.14 |
| 64 | 81.0 | 9.01 | 117.49 |
| 70 | 80.3 | 9.61 | 142.67 |

of optical signals in underwater media. These can corrupt the transmitted data and create errors in the packets. Error-correcting codes are utilized throughout digital communication systems. The idea behind these codes is to add redundancy bits to the original bits before transmission. Therefore, while passing through this analog channel, where the signal is exposed to noise, the original packet may be corrupted before it reaches the receiver. The added redundancy in the error-correcting code will enable the receiver to detect (to some degree) and possibly correct errors caused by the attenuation and scintillation in the signal using clever algorithms. BCH codes operate over Galois fields (GFs) [56]. The detailed encoding and decoding structures of BCH codes are explained using a polynomial structure.

### A. BCH (31, 16) ENCODER

The elements of the field $GF\left(2^5\right)$ are $\{0, 1, \alpha, \alpha^2, \ldots, \alpha^{30}\}$, where $\alpha$ is a primitive element of $GF(2^5)$. The generator polynomial $g(x)$ is used to obtain the coded polynomial using the minimal polynomials formed by the conjugate classes of the elements of the GF. The conjugate classes and corresponding minimal polynomials of the $GF(2^5)$ field are given in [44]. Let $\phi_i(x)$ be the minimal polynomial of $\alpha^i$. The generator polynomial $g(x)$ is obtained using the least common multiple

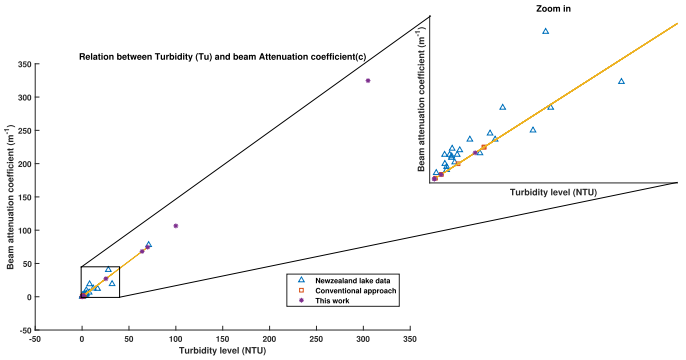


**FIGURE 5.** Relationship between the beam attenuation coefficient and turbidity levels.

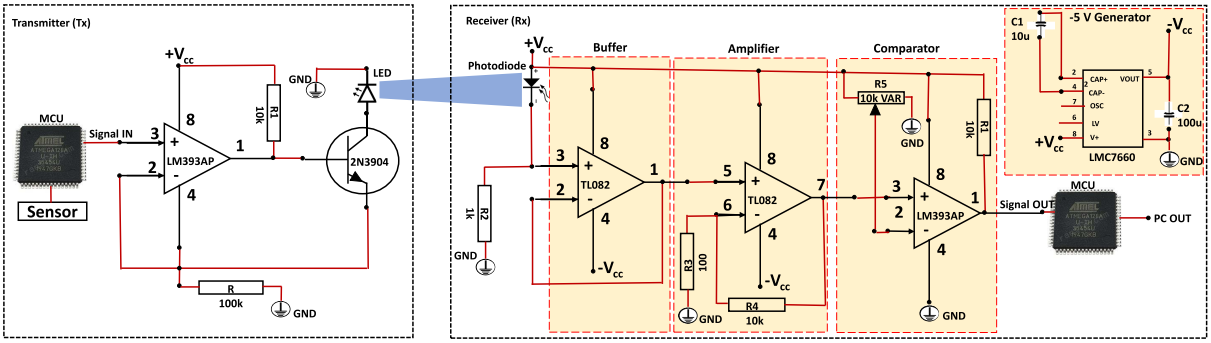


**FIGURE 6.** Circuit diagram of transmitter and receiver sections.

of $\phi_1(x), \phi_2(x), \ldots, \phi_{2t}(x)$, where $t$ represents the correction capability of the error-correcting bits [57].

The generator polynomial of a BCH code with $t = 3$ (3-bit error-correcting capability) is obtained using

$$g(x) = \{\phi_1(x)\phi_3(x)\phi_5(x)\} \tag{1}$$

where $\phi_1(x) = x^5+x^2+1$, $\phi_3(x) = x^5+x^4+x^3+x^2+1$, and $\phi_5(x) = x^5+x^4+x^2+x+1$ are the minimal polynomials of the $\alpha$, $\alpha^3$, and $\alpha^5$ conjugate classes, respectively. Substitution of the minimal polynomials, binomial addition of the base, and decimal addition and multiplication of the powers of the polynomials yields the generator polynomial

$$g(x) = x^{15} + x^{11} + x^{10} + x^9 + x^8 + x^7 + x^5 + x^3 + x^2 + x + 1, \tag{2}$$

The code-word polynomial is obtained by multiplying the generator polynomial by the information polynomial, *i.e.*, $c(x) = g(x) \times m(x)$, where $m(x)$ is the information message polynomial, obtained as $m = [m_0, m_1, \ldots, m_{15}] = m_0 + m_1x + m_2x^2 + \cdots + m_{15}x^{15}$. The systematic $(n, k)$ encoding is obtained using

$$c(x) = r(x) + x^{n-k}m(x), \tag{3}$$

where $n$ is the code-word length, $k$ is the length of the information bits, and $r(x)$ is the remainder polynomial obtained when dividing $x^{n-k}m(x)$ by the generator polynomial $g(x)$.

The coefficients of the code-word polynomials are modulated with the LED source, and the modulated optical beam is communicated through the underwater columns using a plano-convex collimating lens.The LFSR architecture for BCH (31, 16) encoding, obtained using the generator polynomial $g(x) = x^{15}+x^{11}+x^{10}+x^9+x^8+x^7+x^5+x^3+x^2+x+1$, is illustrated in figure 7.

### B. BCH (31, 16) DECODER

At the receiver, the data obtained using the photodetector consist of redundancy bits and noisy versions of the information bits. The decoder plays an important role in the forward error control codes. In this paper, we decode the noisy received data using the Berlekamp-Massey algorithm.

1) Generate the elements of the GF GF($2^5$) with respect to the primitive polynomial $p(x) = x^5 + x^2 + 1$.
2) Generate the syndrome polynomial from the $2t$ syndrome results. The equations of the syndromes (for $(1 \leq j \leq 2t)$) and the syndrome polynomial with all the syndromes as coefficients are

$$S_j = \sum_{i=0}^{n-1} R_i \alpha^{i-j}$$

and

$$S(x) = S_1x + S_2x + \cdots + S_{2t}x^{2t}.$$

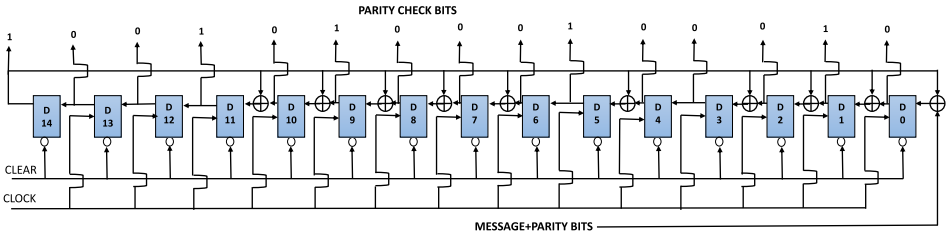


**FIGURE 7.** LFSR architecture for g(x).

3) Run Berlekamp's algorithm iteratively to search for the error locator polynomial solution $\Lambda^{2k}(x)$.

$$[1 + S(x)]\Lambda^{2k}(x) \equiv (1 + \Omega_2 x^2 + \Omega_4 x^4 + \cdots\cdots + \Omega_{2k} x^{2k+1}),$$

where k is 1 to t and $\Omega_j$ is the coefficient of the error locator polynomial.

#### 1) BERLEKAMP BINARY BCH DECODING ALGORITHM

1) Calculate the syndrome $S_i = R(\alpha^i)$, and form the syndrome polynomial $S(x) = S_1 x + S_2 x + \cdots + S_{2t} x^{2t}$, where $R(x) = 1 + R_1 x + R_2 x + \cdots + R_{n-1} x^{n-1}$ is the received polynomial.
2) Initialize with $\Lambda^{(0)}(x) = 1, k = 0, and T^{(0)}(x) = 1$.
3) Let $\Delta^{(2k)}$ be the coefficient of $x^{2k+1}$ in the resultant product $[1 + S(x)]\Lambda^{2k}(x)$.
4) Compute

$$\Lambda^{2k+2}(x) = \Lambda^{2k}(x) + \Delta^{(2k)}[x.T^{(2k)}(x)].$$

5) Calculate

$$T^{(2k)}(x) = \begin{cases} x^2 T^{(2k)}(x) & \begin{cases} \text{if } \deg[\Lambda^{(2k)}(x)] \\ > k \text{ or if } \Delta^{(2k)} = 0 \end{cases} \\ (x\Lambda^{(2k)}(x))/\Delta^{(2k)} & \begin{cases} \text{if } \deg[\Lambda^{(2k)}(x)] \\ \leq k \text{ and if } \Delta^{(2k)} \neq 0. \end{cases} \end{cases}$$

6) Increment k (k = k + 1). If k < t, loop back to step 3.
7) Check the roots of $\Lambda(x) = \Lambda^{2t+2}(x)$. The algorithm works when the roots are distinct and within the GF. Therefore, if the proper roots meet the required conditions, flip the bits corresponding to the error location(s). Otherwise, the algorithm will not correct all the errors in the packet.

### C. SOFTWARE IMPLEMENTATION

Considering the node design constraints, mobility requirement, and the limitation of the processing power of the MCU, a triple-error-correcting binary BCH (31, 16) block code is implemented. The encoder/decoder are wholly software based algorithms which enable the interface to be less complex, compact, and more efficient. This enable the transmitter/sensor interface to encode/process the message data on-board without the extension of any third party resources. The information to be transmitted is split into blocks of a certain length, and each block is encoded and decoded independently of the other blocks. The number 31 is the length of each block (in bits), and the number 16 is the number of information bits per block. Therefore, BCH (31, 16) has 31 - 16 = 15 redundancy bits per 31-bit block, or approximately 50%. The efficiency of the code increases with the number of redundancy bits, but this reduces the data rate. Therefore, the trade-off between the efficiency and the data rate should be considered a design constraint. The elements of the GF($2^5$) corresponding to the primitive polynomial $p(x) = x^5 + x^2 + 1$ are generated using Matlab and stored in separate arrays on the encoder and the decoder as a lookup table and a reverse lookup table, respectively. Each lookup table comprises of 32 characters. The character value in the table represents the corresponding value of the power of alpha. The program design can be divided into two main portions.

#### 1) ENCODING OF MESSAGE BITS

Since the BCH codes operate over the GF, all the mathematical operations (addition, multiplication, and division) are solved over the finite binary field GF(2). This advantage makes the XOR function extremely useful in solving finite arithmetic fields.

- The message string to be transmitted is stored in its specified array in the micro-controller. The encoding algorithm is applied to this message string to generate the code-word and send it to the transmitter.
- The encoder function takes two characters (16 bits) from the message string and converts the message into a 32-bit unsigned long variable after the encoding.
- The code-word is obtained by left-shifting the 16-bit message by the degree (31 ? 16 = 15) of the generator polynomial g(x), and the result is added to the remainder.
- The remainder is calculated by dividing the shifted result by the generator polynomial.

#### 2) DECODING OF MESSAGE BITS

- The received message is stored in a 32-bit long array. The decoder function takes this long variable and computes the six syndrome values.
- The syndrome values are calculated at six different powers of alpha, namely, the primitive elements in the

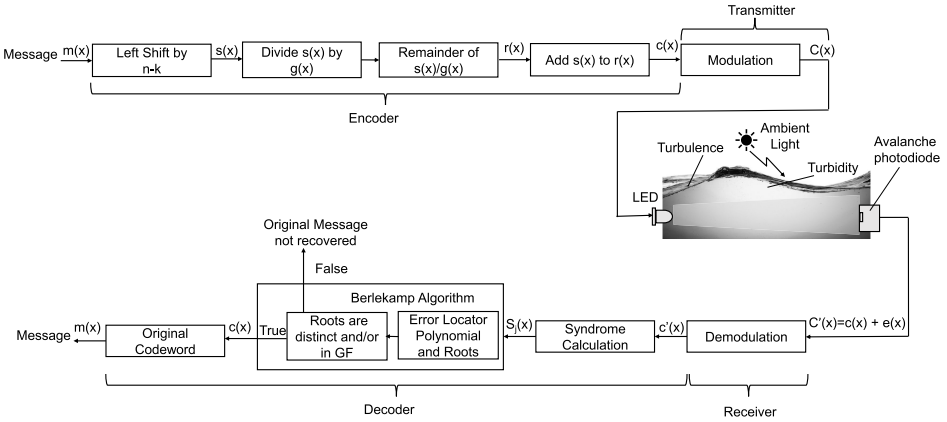


**FIGURE 8.** Schematic of software portion (encoder/decoder) of transmitter/receiver.

GF($2^5$), which are saved in the lookup table and stored in an array in the micro-controller.

- The decoder function takes these syndrome values to calculate the syndrome polynomial before calling Berlekamp's algorithm.
- Berlekamp's algorithm looks for the polynomial; the error can be located by evaluating the syndrome polynomial iteratively.
- If there are errors in the received message and the limits of the BCH code, i.e., $t \leq 3$, Berlekamp's algorithm will produce the error locator polynomial.
- The error locator polynomial is assessed to find the location of the roots and error(s). The validity of the roots is then quantified.
- If the roots are distinct and within the right field, the corresponding bit(s) of the locator polynomial will be flipped to correct the corrupted bit(s).

Figure 8 illustrates the software implementation of the encoder and the decoder of the system.

## VII. EXPERIMENTAL RESULTS AND DISCUSSION

In the proposed UWOC system, the information bit stream is encoded at the transmitter and then modulated using LEDs with wavelengths of 470 and 730 nm. The modulated optical signal is propagated through the water. The data frame consists of two synchronization bytes, namely, 16 information bits and 15 redundancy bits, and 8 stop bits for detecting the end of the data frame, as shown in figure 9. The uncoded system can achieve a 90% PSR at a maximum luminous intensity of about 830 lux. Hence, the ambient light is fixed at 810-830 lux during this set of experiments. The effects of ambient light in the water are studied and analyzed by exposing the water to sunlight and ambient light from an 810-830 lux LED panel. Live waves, namely, constant turbulence of 5 L/min, are generated in the water channel using a pump to emulate the physical environment and disturbance inside a small pond and study the effect of turbulence. The experiment is conducted in clean water with a turbidity level of 0.1 NTU. The received optical signal is detected using photo-diodes

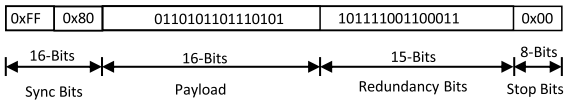


**FIGURE 9.** Example of transmitted signal block (data frame).

**TABLE 3.** Experimental parameters used in evaluation.

| | | | | |
|---|---|---|---|---|
| Transmitter | Power Source (DC) | | | 5 V |
| | LED | Power (mW) | Blue ($\lambda$=470 nm) | 102 |
| | | | Red ($\lambda$=730 nm) | 72 |
| | | Luminous Intensity (mcd) | | 2500 |
| | | Luminous Flux (lm) | Blue ($\lambda$=470 nm) | 1.5 |
| | | | Red ($\lambda$=730 nm) | 2.5 |
| | | Wave Length ($\lambda$) (nm) | Blue | 470 |
| | | | Red | 730 |
| Channel | Water Pump (Displacement Rate (L/min)) | | | 5 |
| | Lighting Intensity (surroundings) (lux) | | | 810-830 |
| | Turbidity (NTU) | | | 0.1-5 |
| | Distance (m) | | | 4 |
| Receiver | Data Rate (Kbps) | | | 2.4-115.2 |
| | PD | Photosensitive Area ($mm^2$ ) | SiPIN | 10x10 |
| | | | MPPC-APD | 6x6 |
| | | Peak Sensitivity Wavelength ($\lambda_p$) (nm) | SiPIN | 960 |
| | | | MPPC-APD | 450 |

(a Si-PIN [S5107] and an MPPC [S13360]). The optical signal is then converted into an electrical signal using an appropriate circuit. An ATmega128A with an operating voltage of 12 V (minimum of 3.7 V) and current of 1 mA is used to demodulate the received electrical pulses and decode the information bits. The experimental parameters used in the experiment are given in table 3.

Figures 10a and 10b demonstrate the experimental results for the UWOC system without BCH coding at LED wavelengths of 470 and 730 nm, respectively. The graphs show that the combination of ambient light and turbulence can cause a severe disturbance in the water channel, resulting in packet loss and errors. As the transmission data rate increases, the number of successfully received packets decreases. At a data

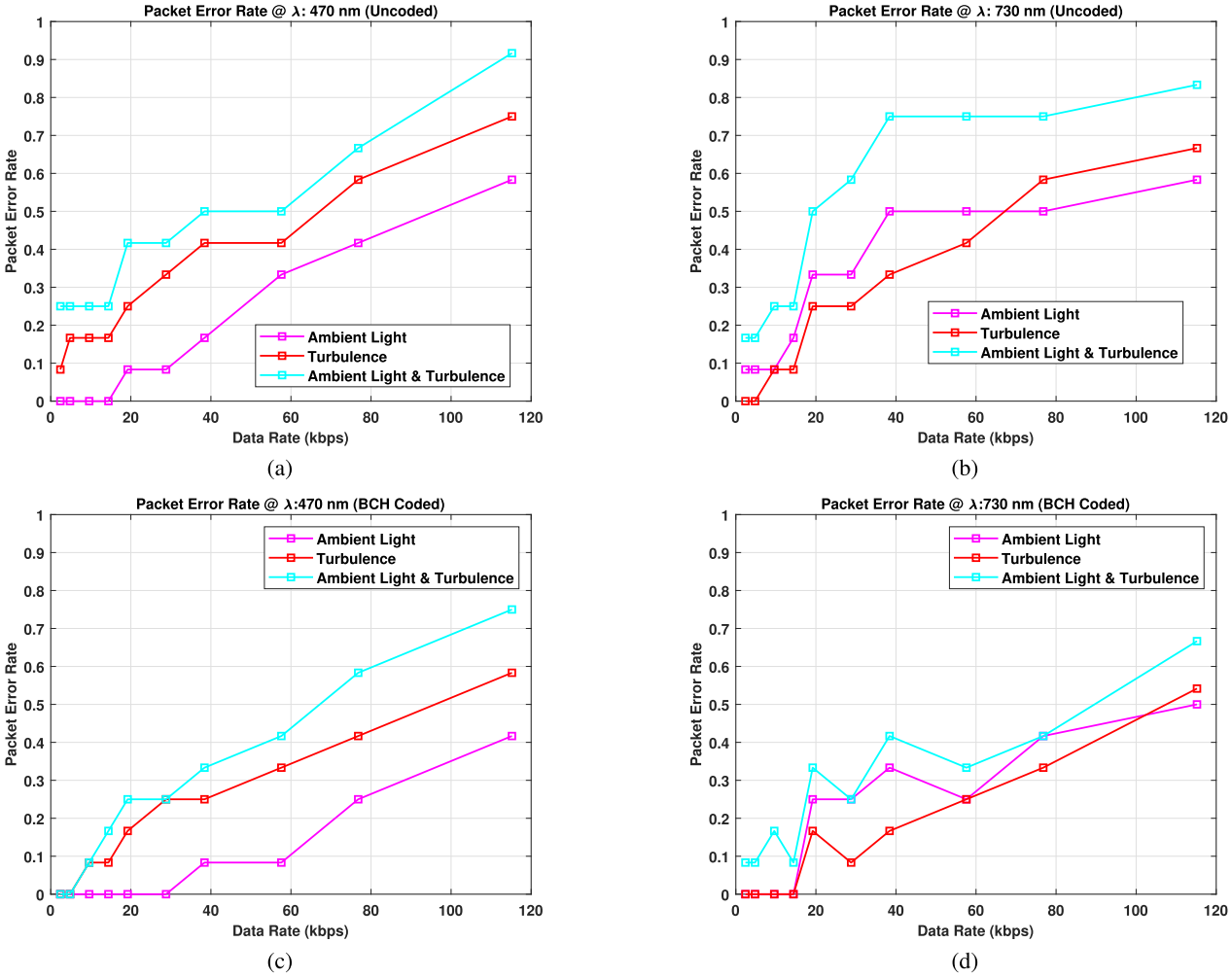


**FIGURE 10.** PERs of UWOC systems under high ambient light, water turbulence, and combined light and turbulence: (a) (b) uncoded UWOC system, (c) (d) BCH-coded UWOC system.

rate of 2.4 Kbps, approximately 42% and 50% of packets are lost or corrupted at the wavelengths of 470 nm (blue) and 730 nm (red), respectively, due to the combined effect of ambient light and turbulence in the water channel. Furthermore, the performance of the UWOC system declines as the data rate increases. The accumulated effect of the 830 lux ambient light and the induced turbulence results in PERs of about 90% and 85% at 470 and 730 nm, respectively. Figures 10c and 10d show the experimental results for the BCH-coded UWOC system operating at 470 and 730 nm, respectively. These findings are obtained after exposing the system to about 830 lux of surrounding ambient light, as measured at the center of the water tank. Turbulence is also induced in the water tank to analyze the combined effect of light and turbulence on the LED-powered, BCH-coded UWOC system. The performance of the system is enhanced, and the BCH code exhibits a good improvement in recovering or correcting lost or corrupted packets. The performance of the proposed system with respect to the PER is compared in table 4.

A comparison between the uncoded and BCH-coded UWOC systems indicates that the packet loss is much smaller in the BCH-coded UWOC system. Figures 10c and 10d show that the system performance of the BCH-coded system is better by 12% and 11% than that of the uncoded system powered with the blue LED at the data rates of 115.5 and 2.4 Kbps, respectively. The BCH-enabled UWOC system with the optical signal of 730 nm shows performance improvements of 20% and 11% in recovering corrupted packets compared with the uncoded system at 2.4 and 115.5 Kbps, respectively. This is a promising result for the proposed BCH-coded UWOC system. The percentages of performance improvement suggest that the channel is not deterministic, as the PER enhancement for the BCH-coded link operating at 470 and 730 nm fluctuates between 7%-25% and 1%-42%, respectively. As seen in figure 10, both the optical signals (470 and 730 nm) are suitable for a UWOC system with clean tap water.

System performance is evaluated regarding the distance between the transmitter node and the receiver using the

**TABLE 4.** Performance of BCH-coded UWOC system.

| Data Rate (Kbps) | Packet Error Rate (%) | | | | | |
|---|---|---|---|---|---|---|
| | Blue LED ($\lambda$: 470 nm) | | | Red LED ($\lambda$: 730 nm) | | |
| | Uncoded (%) | Coded (%) | Improvement (%) | Uncoded (%) | Coded (%) | Improvement (%) |
| 2.4 | 25 | 0 | 25 | 17 | 9 | 8 |
| 4.8 | 25 | 0 | 25 | 17 | 8 | 7 |
| 9.6 | 25 | 9 | 16 | 25 | 24 | 1 |
| 14.4 | 25 | 17 | 8 | 25 | 9 | 16 |
| 19.2 | 41 | 25 | 16 | 50 | 34 | 16 |
| 28.8 | 41 | 25 | 16 | 58 | 25 | 33 |
| 38.4 | 50 | 34 | 16 | 75 | 42 | 33 |
| 57.6 | 50 | 41 | 9 | 75 | 33 | 42 |
| 78.8 | 66 | 59 | 7 | 75 | 42 | 33 |
| 115.2 | 92 | 75 | 17 | 83 | 67 | 16 |

**TABLE 5.** Experimental parameters used in evaluation.

| | | | |
|---|---|---|---|
| Transmitter | DC Power Battery | | 5 V |
| | LED | Power (mW) | 102 |
| | | Luminous Intensity (mcd) | 2500 |
| | | Luminous Flux (lm) | 1.5 |
| | | Wavelength ($\lambda$) | 470 |
| Channel | Aerating Jets | Airflow rate (L/min) | 2.5 |
| | | No. of outlets | 2 |
| | Water Pump (Displacement Rate (L/min)) | | 5 |
| | Lighting Intensity (surroundings) (lux) | | 1500-1550 |
| | Turbidity (NTU) | | 0.1-1320 |
| Receiver | Data Rate (Kbps) | | 19.2 |
| | Si-PIN PD | Photosensitive Area ($mm^2$) | 10x10 |
| | | Peak Sensitivity Wavelength ($\lambda_p$) (nm) | 960 |

waterproof experimental box shown in figure 4. The microcontroller (ATmega128A) and the transmitter are powered by a 5 V Li-Po battery with a 1 mA current. The blue LED used in this experiment has a luminous intensity of 2500 mcd, power of 102 mW, and wavelength of 470 nm. The data transmission rate during this experiment is kept constant at 19,200 bps. In the experiments, the concentration of the air bubble population is varied, ZnO powder is used to make the water turbid to different degrees, and turbulence is generated with a pump to emulate the turbulent waves in natural water environments. The experimental parameters are given in table 5.

Figure 11 shows the PSRs versus changes in turbidity and air bubble population. Figure 11a depicts the system's performance at a turbidity of 0.1 NTU. The result shows that the system can achieve a range of up to 3 m with a 10% PSR without the BCH code, but the PSR improves to 20% with the use of the BCH-coded link. According to figures 11b and 11c, the system can maintain communication up to 2 and 1 m at turbidity levels of 305 and 1320 NTU, respectively, with PSR improvements of 10% and 3%, respectively.

Figure 11d shows the performance of the system in the presence of the air bubble population. In this experiment, the turbidity of the water is 305 NTU, and the transmitter is positioned 2 m away from the receiver. Table 5 lists the experimental parameters used in this evaluation except the fixed parameters, namely, turbidity and link range. The optical signal power diminishes exponentially past 2.5 m, in which case the received corrupted packets cannot be corrected. As the airflow rate of the aerating jet increases from 1 to 2.5 L/min, the PSR of the uncoded system decreases from 70% to 30%. The PSR is then improved by 10% with the introduction of the BCH-coded link to the UWOC system. The performance of the BCH-coded UWOC system at different turbidity levels and with different distances between the transmitter and the receiver is given in table 6. The achieved PSRs at different air bubble population rates, induced by varying the airflow rate of the aerating jet, are illustrated in table 7.

The performance of the BCH-coded system is evaluated by varying the turbidity of the water channel according to the turbidity values given in table 2. Extremely low ambient light of about 0-5 lux is applied, turbulence due to small air bubbles is induced by the aerating jet at an airflow rate of 1.2 L/min, and water waves are created by the water pump at a water displacement rate of 2.5 L/min. The data rate and the communication link range of the system are kept constant at 0.5 Mbps and 4 m, respectively, during the evaluation. The parameters used in this experiment are listed in table 8. The PSR performance achieved by the deployed BCH-coded system is compared with that of the uncoded system in figure 12. The achieved PSRs at the varying turbidity levels in the presence of air bubbles, waves, and extremely low surrounding lighting is detailed in table 9. The figure shows that the system exhibits a robust performance at low turbidity levels. The BCH-coded system achieves a 6% improvement compared with the uncoded link at a turbidity level of 64 NTU. Although the PSR performance of both the uncoded and BCH-coded systems is greater than 80% at turbidities of 0-100 NTU, the BCH-coded link further improves system performance by about 3%, 6%, 4%, and 4.5% at the turbidity levels of 25.42, 64, 70, and 100 NTU, respectively, compared with the uncoded system performance.

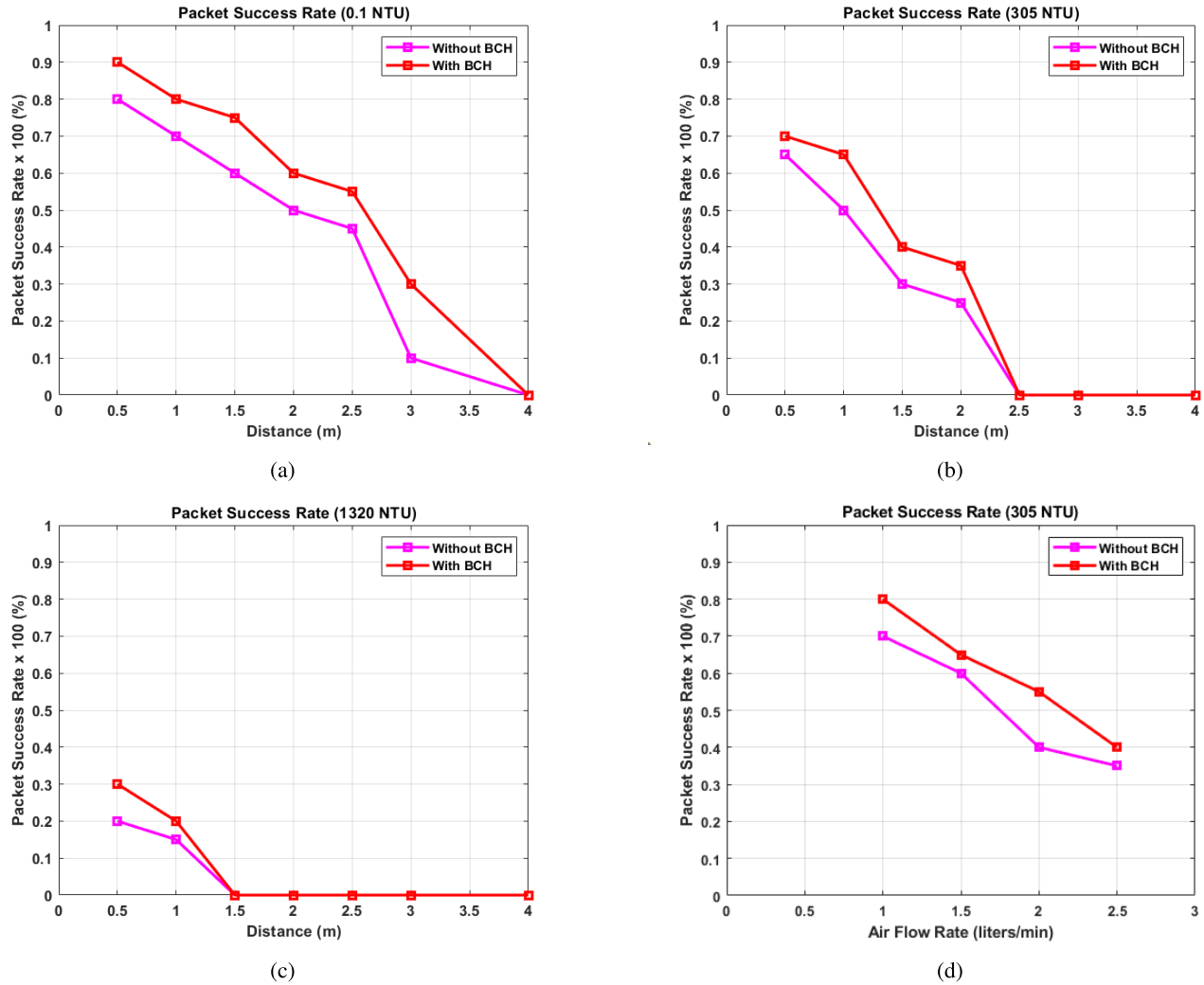


**FIGURE 11.** PSRs against different turbidity levels and bubble populations with varying link distances: (a) 0.1 NTU, (b) 305 NTU, (c) 1320 NTU, (d) 305 NTU.

**TABLE 6.** PSRs of BCH-coded UWOC system at various turbidity levels.

| Distance (m) | PSR (%) | | | | | | | | |
|---|---|---|---|---|---|---|---|---|---|
| | 0.1 NTU | | | 305 NTU | | | 1320 NTU | | |
| | uncoded | Coded | Improvement | uncoded | Coded | Improvement | uncoded | Coded | Improvement |
| 0.5 | 80 | 90 | 10 | 67 | 70 | 3 | 20 | 30 | 10 |
| 1 | 70 | 79 | 9 | 50 | 63 | 13 | 17 | 20 | 3 |
| 1.5 | 69 | 77 | 8 | 30 | 40 | 10 | 0 | 0 | 0 |
| 2 | 50 | 60 | 10 | 27 | 37 | 10 | 0 | 0 | 0 |
| 2.5 | 44 | 58 | 12 | 0 | 0 | 0 | - | - | - |
| 3 | 10 | 30 | 10 | - | - | - | - | - | - |

Moreover, the 0.5 Mbps BCH-assisted system's performance is evaluated in different water types i.e. clear, coastal, harbor I, and harbor II with varying beam attenuation coefficient c. The experiments are conducted in the presence of high ambient light in order of 1550 lux, in addition to the water bubbles population being produced by the aerating jet with the airflow rate of 2.5 liters/min, and the induced wave disturbance by the pump of 5 liters/min displacement rate. Figure 5 is utilized to calculate the corresponding approximate turbidity level with respect to beam attenuation coefficient of different water types. Furthermore, table 10 illustrates the relationship between the beam attenuation coefficient (c), and turbidity level (TU) of different water types. Figure 13 shows the BER performance of the 0.5 Mbps system in different ocean water types at varying communication link distance. The figure clearly shows that the system has achieved better

**TABLE 7. PSRs of BCH-coded UWOC system at various air bubble population rates.**

| Airflow Rate (L/min) | PSR (%) at 305 NTU | | |
|---|---|---|---|
| | Uncoded | Coded | Improvement |
| 1 | 70 | 80 | 10 |
| 1.5 | 60 | 64 | 4 |
| 2 | 40 | 54 | 14 |
| 2.5 | 38 | 40 | 2 |

**TABLE 8. Experimental parameters used in evaluation.**

| | | | |
|---|---|---|---|
| Transmitter | DC Power Battery | | 5 V |
| | LED | Power (mW) | 102 |
| | | Luminous Intensity (mcd) | 2500 |
| | | Luminous Flux (lm) | 1.5 |
| | | Wavelength ($\lambda$) | 470 |
| Channel | Aerating Jets | Airflow rate (L/min) | 1.2 |
| | | No. of outlets | 2 |
| | Water Pump (Displacement Rate (L/min)) | | 2.5 |
| | Lighting Intensity (surroundings) (lux) | | 0-5 |
| | Turbidity (NTU) | | 0.09-100 |
| | Link Range (m) | | 4 |
| Receiver | Data Rate (Mbps) | | 0.5 |
| | SiPIN PD | Photosensitive Area ($mm^2$) | 10x10 |
| | | Peak Sensitivity Wavelength ($\lambda_p$) (nm) | 960 |

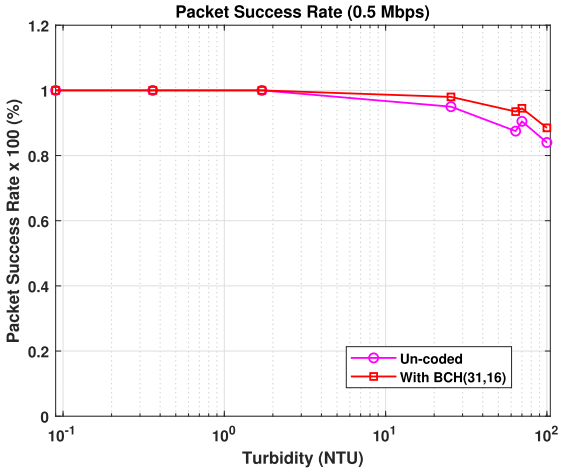


**FIGURE 12. PSRs of BCH-coded and uncoded systems at varying turbidity levels.**

**TABLE 9. PSRs of BCH-coded UWOC system at varying turbidity levels [51].**

| Turbidity (NTU) | PSR (%) at 0.5 Mbps | | |
|---|---|---|---|
| | Uncoded | Coded | Improvement |
| 0.09 | 100 | 100 | - |
| 0.36 | 100 | 100 | - |
| 1.71 | 100 | 100 | - |
| 25.42 | 95 | 98 | 3 |
| 64 | 87.5 | 93.5 | 6 |
| 70 | 90.5 | 94.5 | 4 |
| 100 | 84 | 88.5 | 4.5 |

**TABLE 10. Water types based on measured data from [54], [55] and corresponding turbidity levels.**

| Water types | c ($m^{-1}$) | TU ($NTU$) |
|---|---|---|
| Clear | 0.15 | $\approx 0.14$ |
| Coastal | 0.4 | $\approx 0.38$ |
| Harbor | 2.19 | $\approx 2.06$ |
| Harbor I | 1.1 | $\approx 1.04$ |
| Harbor II | 2.2 | $\approx 2.07$ |

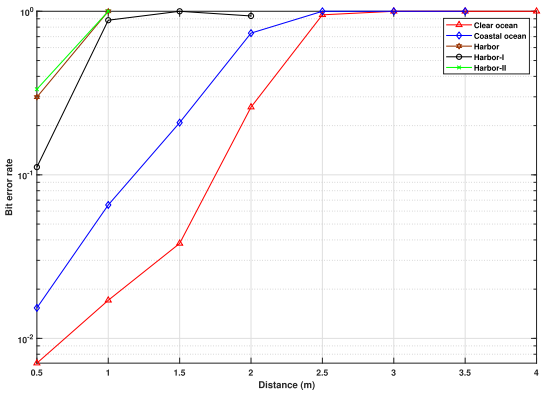


**FIGURE 13. BER performance of the system in different ocean water types.**

performance while operating in clear and coastal water as compared to other ocean water types.

The comparison results of the bit error rates of the uncoded system and various BCH-coded systems are shown in figure 15. The experimental results for all BCH-coded systems in the figure except the BCH (31, 16)-coded system are achieved by utilizing the system mentioned in [30]. A high-level Matlab program is used to encode the message bits into a data packet with the generated redundancy bits for transmission. The encoded packet is stored as a string in the MCU and streamed continuously in an infinite loop with the help of a software-defined modulator. The receiver amplifies and digitizes (demodulation) the received signal for further processing (decoding) in Matlab. The figure shows that the BCH (31, 16) and BCH (31, 11) codes perform comparably well until the communication link range of about 2 m, illustrating their suitability for small underwater LANs. Although the two schemes have an almost similar computational complexity, as shown in figure 16, BCH (31, 16) is preferred for SMP applications because it has more message bits (higher code-word rate) than BCH (31, 11). The parameters used for this evaluation are in table 11. The effect of ambient light and light surrounding the system is analyzed by modifying the data rate and measuring the lux intensity at the receiver end. The experiment is conducted under about 5 lux of surrounding light in the laboratory. The lux intensity is examined by changing the data rate of the optical signal, as shown in figure 14. The lux value is directly proportional to the data rate of the optical signal. The graph is plotted by considering both wavelengths (470 and 730 nm) used in the proposed

**TABLE 11. Experimental parameters used in evaluation.**

| | | | |
|---|---|---|---|
| Transmitter | DC Power Battery | | 5 V |
| | LED | Power (mW) | 102 |
| | | Luminous Intensity (mcd) | 2500 |
| | | Luminous Flux (lm) | 1.5 |
| | | Wavelength ($\lambda$) | 470 |
| Channel | Aerating Jets | Airflow rate (L/min) | 2.5 |
| | | No. of outlets | 2 |
| | Water Pump (Displacement Rate (L/min)) | | 5 |
| | Lighting Intensity (surroundings) (lux) | | 800-830 |
| | Turbidity (NTU) | | 25 |
| Receiver | Data Rate (Kbps) | | 230.4 |
| | SiPIN PD | Photosensitive Area ($mm^2$) | 10x10 |
| | | Peak Sensitivity Wavelength ($\lambda_p$) (nm) | 960 |

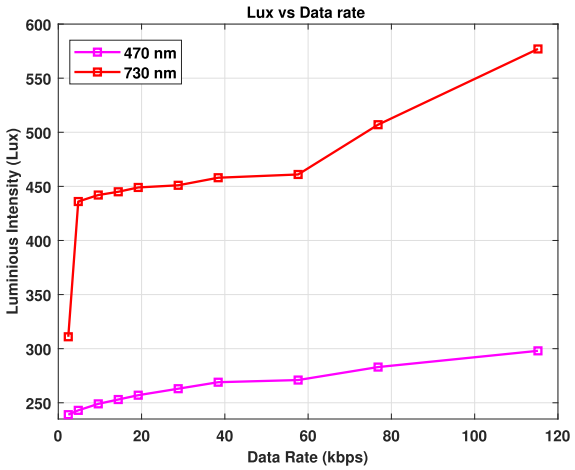


**FIGURE 14. Luminous intensity versus data rate at receiver end.**

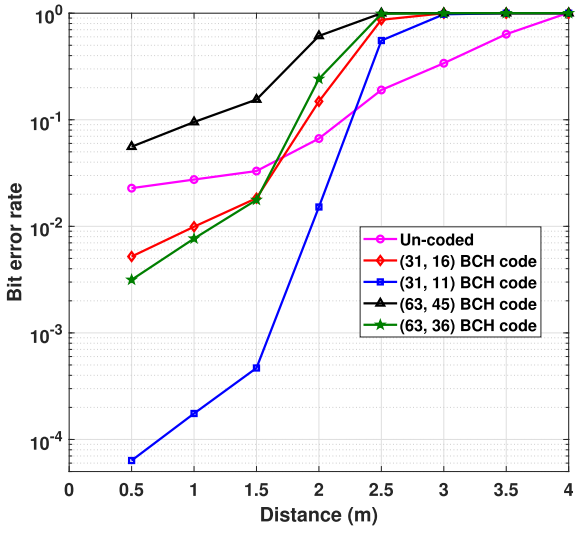


**FIGURE 15. Bit error rates of BCH-coded and uncoded systems.**

work. The luminous intensity of the red LED (730 nm) is relatively higher than that of the blue LED (470 nm).

### A. COMPLEXITY ANALYSIS

The computational complexities of different BCH encoders and decoders are obtained using the number of multiplications

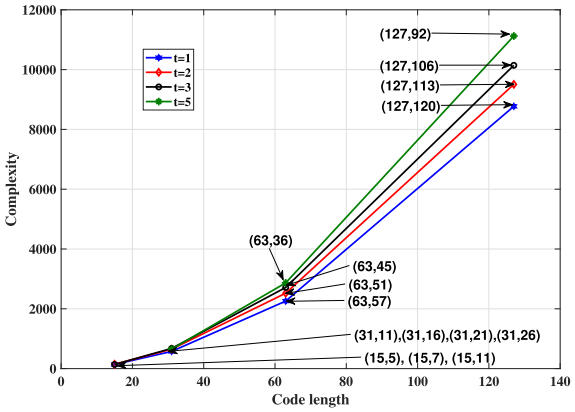


**FIGURE 16. Computational complexities of various BCH codes.**

in each code. For an $(n, k)$ BCH code, the encoder performs $(n-k)(k-1)$ multiplications, and Berlekamp-Massey solves $2\lfloor\frac{n^2}{4}\rfloor - n + 1$. The computational complexity of the studied BCH codes in 1-, 2-, and 3-bit error correction is shown in figure 16.

## VIII. CONCLUSION

In this article, a BCH-coded UWOC system is proposed to mitigate the effects of turbulence, absorption, and scattering in underwater channels on low-power sensor nodes. The proposed UWOC system is designed to evaluate different parameters in UWOC. The circuit is constructed, and physical demonstrations are performed in an experimental setup resembling a natural aquatic environment. The performance of the proposed power-efficient UWOC system is evaluated under different lighting, turbulence, and turbidity conditions. Its performance is also assessed in the presence of varying concentrations of air bubbles. The BCH-coded system shows promising results in reconstructing the optimal quantity of corrupted packets.

## REFERENCES

[1] O. Gupta, N. Goyal, D. Anand, S. Kadry, Y. Nam, and A. Singh, "Underwater networked wireless sensor data collection for computational intelligence techniques: Issues, challenges, and approaches," *IEEE Access*, vol. 8, pp. 122959–122974, 2020.
[2] M. Stojanovic, "Recent advances in high-speed underwater acoustic communications," *IEEE J. Ocean. Eng.*, vol. 21, no. 2, pp. 125–136, Apr. 1996.
[3] M. Chitre, S. Shahabudeen, and M. Stojanovic, "Underwater acoustic communications and networking: Recent advances and future challenges," *Mar. Technol. Soc. J.*, vol. 42, no. 1, p. 103, 2008.
[4] I. F. Akyildiz, D. Pompili, and T. Melodia, "Underwater acoustic sensor networks: Research challenges," *Ad Hoc Netw.*, vol. 3, no. 3, pp. 257–279, Mar. 2005.
[5] T. Oberg, B. Nilsson, N. Olofsson, M. L. Nordenvaad, and E. Sangfelt, "Underwater communication link with iterative equalization," in *Proc. OCEANS*, Sep. 2006, pp. 1–6.
[6] M. Chitre, S. Shahabudeen, L. Freitag, and M. Stojanovic, "Recent advances in underwater acoustic communications networking," in *Proc. OCEANS*, 2008, pp. 1–10.
[7] I. F. Akyildiz, P. Wang, and Z. Sun, "Realizing underwater communication through magnetic induction," *IEEE Commun. Mag.*, vol. 53, no. 11, pp. 42–48, Nov. 2015.
[8] H. M. Oubei, C. Shen, A. Kammoun, E. Zedini, K. H. Park, X. Sun, G. Liu, C. H. Kang, T. K. Ng, M. S. Alouini, and B. S. Ooi, "Light based underwater wireless communications," *Jpn. J. Appl. Phys.*, vol. 57, no. 8S2, 2018, Art. no. 08PA06.

[9] H. Kaushal and G. Kaddoum, "Underwater optical wireless communication," *IEEE Access*, vol. 4, pp. 1518–1547, 2016.
[10] M. Tivey, P. Fucile, and E. Sichel, "A low power, low cost, underwater optical communication system," Ridge 2000 Events, Arlington, TX, USA, Apr. 2004, pp. 27–29.
[11] S. Tang, Y. Dong, and X. Zhang, "Impulse response modeling for underwater wireless optical communication links," *IEEE Trans. Commun.*, vol. 62, no. 1, pp. 226–234, Jan. 2013.
[12] V. Guerra, J. Rufo, J. Rabadan, and R. Perez-Jimenez, "Effect of moving microalgae on underwater wireless optical links," *Appl. Opt.*, vol. 59, no. 2, pp. 515–520, 2020.
[13] D. R. K. Mary, E. Ko, S.-G. Kim, S.-H. Yum, S.-Y. Shin, and S.-H. Park, "A systematic review on recent trends, challenges, privacy and security issues of underwater Internet of Things," *Sensors*, vol. 21, no. 24, p. 8262, Dec. 2021.
[14] M. Doniec, A. Xu, and D. Rus, "Robust real-time underwater digital video streaming using optical communication," in *Proc. IEEE Int. Conf. Robot. Automat.*, May 2013, pp. 5117–5124.
[15] J. A. Simpson, W. C. Cox, J. R. Krier, B. Cochenour, B. L. Hughes, and J. F. Muth, "5 Mbps optical wireless communication with error correction coding for underwater sensor nodes," in *Proc. OCEANS MTS/IEEE SEATTLE*, Sep. 2010, pp. 1–4.
[16] M. Singh, M. L. Singh, and R. Singh, "Performance enhancement of 112 Gbps UWOC link by mitigating the air bubbles induced turbulence with coherent detection MIMO DP-16QAM and advanced digital signal processing," *Optik*, vol. 259, Jun. 2022, Art. no. 168986.
[17] B. Shihada, O. Amin, C. Bainbridge, S. Jardak, O. Alkhazragi, T. K. Ng, B. Ooi, M. Berumen, and M. S. Alouini, "Aqua-Fi: Delivering internet underwater using wireless optical networks," *IEEE Commun. Mag.*, vol. 58, no. 5, pp. 84–89, May 2020.
[18] S. Chen, J. L. Song, Z. M. Yuan, Y. Liu, and P. P. Guo, "Diver communication system based on underwater optical communication," *Appl. Mech. Mater.*, vol. 621, pp. 259–263, Aug. 2014.
[19] J. W. Giles and I. N. Bankman, "Underwater optical communications systems. Part 2: Basic design considerations," in *Proc. IEEE Mil. Commun. Conf. (MILCOM)*, Oct. 2005, pp. 1700–1705.
[20] J. H. Smart, "Underwater optical communications systems. Part 1: Variability of water optical parameters," in *Proc. IEEE Mil. Commun. Conf. (MILCOM)*, Oct. 2005, pp. 1140–1146.
[21] M. W. Kong, Y. Chen, R. Sarwar, B. Sun, Z. Xu, J. Han, J. Chen, H. Qin, and J. Xu, "Underwater wireless optical communication using an arrayed transmitter/receiver and optical superimposition-based PAM-4 signal," *Opt. Exp.*, vol. 26, no. 3, pp. 3087–3097, 2018.
[22] P. Tian, X. Liu, S. Yi, Y. Huang, S. Zhang, X. Zhou, L. Hu, L. Zheng, and R. Liu, "High-speed underwater optical wireless communication using a blue GaN-based micro-LED," *Opt. Exp.*, vol. 25, no. 2, pp. 1193–1201, Jan. 2017.
[23] Y. Zhao, A. Wang, L. Zhu, W. Lv, J. Xu, S. Li, and J. Wang, "Performance evaluation of underwater optical communications using spatial modes subjected to bubbles and obstructions," *Opt. Lett.*, vol. 42, no. 22, pp. 4699–4702, 2017.
[24] H. M. Oubei, R. T. ElAfandy, K.-H. Park, T. K. Ng, M.-S. Alouini, and B. S. Ooi, "Performance evaluation of underwater wireless optical communications links in the presence of different air bubble populations," *IEEE Photon. J.*, vol. 9, no. 2, pp. 1–9, Apr. 2017.
[25] S. Kumar, S. Prince, J. V. Aravind, and G. Santosh Kumar, "Analysis on the effect of salinity in underwater wireless optical communication," *Mar. Georesources Geotechnol.*, vol. 38, no. 3, pp. 291–301, Mar. 2020.
[26] X. Sun, M. Kong, O. Alkhazragi, C. Shen, E.-N. Ooi, X. Zhang, U. Buttner, T. K. Ng, and B. S. Ooi, "Non-line-of-sight methodology for high-speed wireless optical communication in highly turbid water," *Opt. Commun.*, vol. 461, Apr. 2020, Art. no. 125264.
[27] W. Wei, C. Zhang, W. Zhang, W. Jiang, C. Shu, and Q. Xiaorui, "LED-based underwater wireless optical communication for small mobile platforms: Experimental channel study in highly-turbid lake water," *IEEE Access*, vol. 8, pp. 169304–169313, 2020.
[28] Y. Guo, A. Trichili, O. Alkhazragi, I. Ashry, T. K. Ng, M.-S. Alouini, and B. S. Ooi, "On the reciprocity of underwater turbulent channels," *IEEE Photon. J.*, vol. 11, no. 2, pp. 1–9, Apr. 2019.
[29] M. Kong, Y. Guo, O. Alkhazragi, M. Sait, C. H. Kang, T. K. Ng, and B. S. Ooi, "Real-time optical-wireless video surveillance system for high visual-fidelity underwater monitoring," *IEEE Photon. J.*, vol. 14, no. 2, pp. 1–9, Apr. 2022.
[30] W. C. Cox, J. A. Simpson, C. P. Domizioli, J. F. Muth, and B. L. Hughes, "An underwater optical communication system implementing Reed–Solomon channel coding," in *Proc. OCEANS*, 2008, pp. 1–6.
[31] F. Mattoussi, M. A. Khalighi, and S. Bourennane, "Improving the performance of underwater wireless optical communication links by channel coding," *Appl. Opt.*, vol. 57, no. 9, pp. 2115–2120, 2018.
[32] J. A. Simpson, B. L. Hughes, and J. F. Muth, "Smart transmitters and receivers for underwater free-space optical communication," *IEEE J. Sel. Areas Commun.*, vol. 30, no. 5, pp. 964–974, Jun. 2012.
[33] C. Pontbriand, N. Farr, J. Ware, J. Preisig, and H. Popenoe, "Diffuse high-bandwidth optical communications," in *Proc. OCEANS*, 2008, pp. 1–4.
[34] M. Doniec, I. Vasilescu, M. Chitre, C. Detweiler, M. Hoffmann-Kuhnt, and D. Rus, "AquaOptical: A lightweight device for high-rate long-range underwater point-to-point communication," in *Proc. OCEANS*, Oct. 2009, pp. 1–6.
[35] N. Farr, A. D. Chave, L. Freitag, J. Preisig, S. N. White, D. Yoerger, and F. Sonnichsen, "Optical modem technology for seafloor observatories," in *Proc. OCEANS*, Sep. 2005, pp. 928–934.
[36] D. Anguita, D. Brizzolara, and G. Parodi, "Optical wireless communication for underwater wireless sensor networks: Hardware modules and circuits design and implementation," in *Proc. OCEANS MTS/IEEE SEATTLE*, Sep. 2010, pp. 1–8.
[37] F. Akhoundi, J. A. Salehi, and A. Tashakori, "Cellular underwater wireless optical CDMA network: Performance analysis and implementation concepts," *IEEE Trans. Commun.*, vol. 63, no. 3, pp. 882–891, Mar. 2015.
[38] X. Tang, R. Kumar, C. Sun, L. Zhang, Z. Chen, R. Jiang, H. Wang, and A. Zhang, "Towards underwater coherent optical wireless communications using a simplified detection scheme," *Opt. Exp.*, vol. 29, no. 13, pp. 19340–19351, 2021.
[39] C. Wang, H. Y. Yu, and Y. J. Zhu, "A long distance underwater visible light communication system with single photon avalanche diode," *IEEE Photon. J.*, vol. 8, no. 5, pp. 1–11, Oct. 2016.
[40] M. Sun, B. Zheng, L. Zhao, X. Zhao, and F. Kong, "A design of the video transmission based on the underwater laser communication," in *Proc. Oceans-St. John's*, Sep. 2014, pp. 1–4.
[41] A. Al-Halafi, H. M. Oubei, B. S. Ooi, and B. Shihada, "Real-time video transmission over different underwater wireless optical channels using a directly modulated 520 nm laser diode," *IEEE/OSA J. Opt. Commun. Netw.*, vol. 9, no. 10, pp. 826–832, Oct. 2017.
[42] A. Al-Halafi and B. Shihada, "UHD video transmission over bidirectional underwater wireless optical communication," *IEEE Photon. J.*, vol. 10, no. 2, pp. 1–14, Apr. 2018.
[43] X. Yu, W. Jin, M. Sui, and Z. Lan, "Evaluation of forward error correction scheme for underwater wireless optical communication," in *Proc. 3rd Int. Conf. Commun. Mobile Comput.*, Apr. 2011, pp. 527–530.
[44] P. N. Ramavath, S. A. Udupi, and P. Krishnan, "Experimental demonstration and analysis of underwater wireless optical communication link: Design, BCH coded receiver diversity over the turbid and turbulent seawater channels," *Microw. Opt. Technol. Lett.*, vol. 62, no. 6, pp. 2207–2216, Jun. 2020.
[45] M. Doniec, M. Angermann, and D. Rus, "An end-to-end signal strength model for underwater optical communications," *IEEE J. Ocean. Eng.*, vol. 38, no. 4, pp. 743–757, Oct. 2013.
[46] W. C. Cox, K. F. Gray, J. A. Simpson, B. Cochenour, B. L. Hughes, and J. F. Muth, "A MEMS blue/green retroreflecting modulator for underwater optical communications," in *Proc. OCEANS MTS/IEEE SEATTLE*, Sep. 2010, pp. 1–4.
[47] J. S. Everett, "Forward-error correction coding for underwater free-space optical communication," M.S. thesis, Dept. Elect. Eng., North Carolina State Univ., Raleigh, NC, USA, 2009. [Online]. Available: https://repository.lib.ncsu.edu/handle/1840.16/6585
[48] G. Gilbert, T. Stoner, and J. Jernigan, "Underwater experiments on the polarization, coherence, and scattering properties of a pulsed blue-green laser," *Proc. SPIE*, vol. 7, pp. 8–14, Jan. 1966.
[49] K. Liu and Y. Liang, "Underwater image enhancement method based on adaptive attenuation-curve prior," *Opt. Exp.*, vol. 29, no. 7, pp. 10321–10345, 2021.
[50] A. Uppalapati, R. P. Naik, and P. Krishnan, "Analysis of M-QAM modulated underwater wireless optical communication system for reconfigurable UOWSNs employed in river meets ocean scenario," *IEEE Trans. Veh. Technol.*, vol. 69, no. 12, pp. 15244–15252, Dec. 2020.
[51] K. Enhos, E. Demirors, D. Unal, and T. Melodia, "Software-defined visible light networking for Bi-directional wireless communication across the air-water interface," in *Proc. 18th Annu. IEEE Int. Conf. Sens., Commun., Netw. (SECON)*, Jul. 2021, pp. 1–9.

[52] A. S. Trebitz, J. C. Brazner, V. J. Brady, R. Axler, and D. K. Tanner, "Turbidity tolerances of great lakes coastal wetland fishes," *North Amer. J. Fisheries Manage.*, vol. 27, no. 2, pp. 619–633, May 2007.
[53] W. N. Vant and R. J. Davies-Colley, "Factors affecting clarity of New Zealand lakes," *New Zealand J. Mar. Freshwater Res.*, vol. 18, no. 3, pp. 367–377, Sep. 1984.
[54] T. J. Petzold, "Volume scattering functions for selected ocean waters," Scripps Inst. Oceanogr., La Jolla, CA, USA, Tech. Rep. SIO 7278, 1972.
[55] W. Cox and J. Muth, "Simulating channel losses in an underwater optical communication system," *J. Opt. Soc. Amer. A, Opt. Image Sci.*, vol. 31, no. 5, pp. 920–934, 2014.
[56] S. Lin and D. J. Costello, *Error Control Coding*, vol. 2. New York, NY, USA: Prentice-Hall, 2001.
[57] R. Mehra, G. Saini, and S. Singh, "FPGA based high speed BCH encoder for wireless communication applications," in *Proc. Int. Conf. Commun. Syst. Netw. Technol.*, Jun. 2011, pp. 576–579.

**MAAZ SALMAN** received the B.S. degree in telecommunication and information system engineering from the University of Engineering and Technology, Pakistan, in 2017, and the M.S. degree in electrical communication system engineering from Soonchunhyang University, Asan, South Korea. He is currently pursuing the Ph.D. degree in artificial intelligence and convergence with Pukyong National University, South Korea. His research interests include UIoT, underwater sensor networks, underwater optical wireless communication, machine learning assisted IoTs, design of passive microwave components, DGS circuit applications and design, and simulation of RF front end components at microwave and radio spectrum.

**JAVAD BOLBOLI** received the M.Sc. degree from the Amirkabir University of Technology, Tehran, Iran. He is currently pursuing the Ph.D. degree with the Department of Artificial Intelligence Convergence, Pukyong National University, Busan, South Korea. His current research interests include the Internet of Things (IoT), Internet of Underwater Things (IoUT), low-power wide-area networks, and optical wireless communication.

**WAN-YOUNG CHUNG** (Senior Member, IEEE) received the B.Eng. and master's degrees in electronic engineering from Kyungpook National University, Daegu, South Korea, in 1987 and 1989, respectively, and the Ph.D. degree in sensor engineering from Kyushu University, Fukuoka, Japan, in 1998. From 1999 to 2008, he was an Associate Professor at Dongseo University, Busan, South Korea. Currently, he is a Professor with the Department of Electronic Engineering, Pukyong National University, Busan, South Korea. His research interests include wireless sensor networks, ubiquitous healthcare and automobile applications, smart light-emitting systems with visible light communication, and embedded systems. He is the Educational Leader and the Research Group Leader of Artificial Intelligence Convergence, which is supported by the Brain Korea 21 (BK21) Four Project.